British Journal of Pharmacology

DOI:10.1111/j.1476-5381.2010.01068.x
www.brjpharmacol.org

RESEARCH PAPER

Biodistribution, pharmacokinetics and metabolism of interleukin-1 receptor antagonist (IL-1RA) using [^{18}F]-IL1RA and PET imaging in rats

C Cawthorne[1,2]*, C Prenant[1,3]*, A Smigova[1], P Julyan[1,4], R Maroy[5], K Herholz[1], N Rothwell[6] and H Boutin[6]

[1]*Wolfson Molecular Imaging Centre, University of Manchester, Manchester, UK,* [2]*Academic Department of Radiation Oncology, The Christie NHS Foundation Trust, Manchester, UK,* [3]*Cyclopharma, CERRP, Tours, France,* [4]*North Western Medical Physics, Christie Hospital, Manchester, UK,* [5]*SHFJ – CEA, Orsay, France, and* [6]*Faculty of Life Sciences, University of Manchester, Manchester, UK*

Correspondence
Dr Hervé Boutin, Faculty of Life Science, University of Manchester, AV Hill Building, Oxford Road, Manchester M13 9PT, UK. E-mail: herve.boutin@manchester.ac.uk

*Drs Christopher Cawthorne and Christian Prenant contributed equally to this work.

Keywords
IL-1 receptor antagonist; positron emission tomography; biodistribution; metabolism

Received
31 March 2010
Revised
2 September 2010
Accepted
22 September 2010

BACKGROUND AND PURPOSE

Positron emission tomography (PET) has the potential to improve our understanding of the preclinical pharmacokinetics and metabolism of therapeutic agents, and is easily translated to clinical studies in humans. However, studies involving proteins radiolabelled with clinically relevant PET isotopes are currently limited. Here we illustrate the potential of PET imaging in a preclinical study of the biodistribution and metabolism of ^{18}F-labelled IL-1 receptor antagonist ([^{18}F]IL-1RA) using a novel [^{18}F]-radiolabelling technique.

EXPERIMENTAL APPROACH

IL-1RA was radiolabelled by reductive amination on lysine moieties with [^{18}F]fluoroacetaldehyde. Sprague-Dawley rats were injected intravenously with [^{18}F]IL-1RA and imaged with a PET camera for 2 h. For the study of IL-1RA metabolites by *ex vivo* γ-counting of samples, rats were killed 20 min, 1 h or 2 h after injection of [^{18}F]IL-1RA.

KEY RESULTS

[^{18}F]IL-1RA distribution into the major organs of interest was as follows: kidneys >> liver > lungs >> brain. In lungs and liver, [^{18}F]IL-1RA uptake peaked within 1 min post-injection then decreased rapidly to reach a plateau from 10 min post-injection. In the brain, the uptake exhibited slower pharmacokinetics with a smaller post-injection peak and a plateau from 6 min onward. IL-1RA was rapidly metabolized and these metabolites represented ~40% of total activity in plasma and ~80% in urine, 20 min after injection.

CONCLUSIONS AND IMPLICATIONS

Preclinical PET imaging is a feasible method of assessing the biodistribution of new biological compounds of therapeutic interest rapidly. The biodistribution of [^{18}F]IL-1RA reported here is in agreement with an earlier study suggesting low uptake in the normal brain, with rapid metabolism and excretion via the kidneys.

Abbreviations

BBB, blood brain barrier; CSF, cerebrospinal fluid; IL-1, interleukin-1; IL-1RA, IL-1 receptor antagonist; PET, positron emission tomography

Introduction

Studying the pharmacokinetics and metabolism of protein-based therapeutic agents preclinically is labour intensive and expensive in terms of animal use. The use of positron emission tomography (PET) with radiolabelled proteins has been reported before for the RGD peptide (Haubner *et al.*, 2001), somatostatin receptors (Wester *et al.*, 2003), Annexin V (Grierson *et al.*, 2004; Yagle *et al.*, 2005) and affibody for the human epidermal growth factor receptor-2 (Kramer-Marek *et al.*, 2008), but is still not widely used despite the potential to expedite this process by allowing time-course studies, thus reducing the number of animals used and allowing longitudinal studies using disease models. Currently, methods for radiolabelling proteins and peptides with positron-emitting isotopes have limited use for different reasons; the favourable physical and nuclear characteristics of fluorine-18 are accompanied by an adverse time-consuming radiochemistry and the drawback that radiometals (^{64}Cu, ^{66}Ga, ^{68}Ga or ^{86}Y) have much less optimal physical characteristics (half-lives: ^{64}Cu, 12.7h; ^{66}Ga, 9.49 h; ^{86}Y, 14.7 h), low positron-percentage branching (^{64}Cu, 18%; ^{66}Ga, 57%; ^{86}Y, 33%) and high positron energy (^{66}Ga, 1.7MeV; ^{68}Ga, 1.9MeV; ^{86}Y, 1.3MeV) added to co-emission of gamma radiations (^{64}Cu, also 37% of β^-) (Wester and Schottelius, 2007). Consequently, the current impact of protein and peptides labelled with suitable PET isotopes on clinical and preclinical PET studies is still relatively low, and studies of peptides labelled with [^{18}F] are still much rarer than those with SPECT isotopes (Wester and Schottelius, 2007; Schottelius and Wester, 2009). Importantly, proteins labelled with clinically relevant isotopes also offer the potential of translating such studies into man.

The interleukin-1 (IL-1) system has two agonists, IL-1α and IL-1β, and the naturally occurring non-competitive IL-1 receptor antagonist (IL-1RA), all three of which bind to two receptors, namely IL-R1 and IL-1R2 (receptor nomenclature follows Alexander *et al.*, 2009). IL-1 is a well-described pro-inflammatory cytokine that is involved in chronic inflammatory diseases (Freeman and Buchman, 2001; Barksby *et al.*, 2007) such as rheumatoid arthritis (Kavanaugh, 2006), and in neuropathological conditions such as stroke (Touzani *et al.*, 1999; Lee *et al.*, 2004; Pinteaux *et al.*, 2006), Alzheimer's (Holmes *et al.*, 2003; Shaftel *et al.*, 2007), Parkinson's disease (Mogi *et al.*, 1994; Ferrari *et al.*, 2006; Godoy *et al.*, 2008) and epilepsy (Bartfai *et al.*, 2007; Vezzani *et al.*, 2010) (for review, see Simi, *et al.*, 2007; Tansey, *et al.*, 2007; McColl *et al.*, 2009). Both experimental models and clinical studies suggest that IL-1 receptor agonists and their pro-inflammatory actions are detrimental in such neuropathological conditions, whereas IL-1 antagonism seems beneficial (see Allan, *et al.*, 2005 and Lucas *et al.*, 2006). However, some controversy still exists in chronic neurodegenerative conditions such as Alzheimer's (Shaftel *et al.*, 2007; 2008) and Parkinson's diseases (Tansey *et al.*, 2007). These observations have generated interest in developing anti-inflammatory therapeutic strategies targeting the IL-1 system using the naturally occurring IL-1RA.

IL-1RA has proven effective as an anti-inflammatory treatment in several chronic inflammatory diseases (Neven *et al.*, 2010) (see Freeman and Buchman, 2001; Barksby *et al.*, 2007). In parallel, the involvement of IL-1 in stroke led to a phase II clinical trial of IL-1RA in stroke patients which showed that IL-1RA was well tolerated when administered within 6 h of stroke onset (Emsley *et al.*, 2005). Despite the great therapeutic potential of IL-1RA, little has been published about its biodistribution, pharmacokinetics and metabolism. In 1992, Granowitz and colleagues investigated the plasma pharmacokinetics of IL-1RA in healthy volunteers, reporting a short biological half-life of 21 ± 3 min and excretion of intact IL-1RA in the urine (3.2% of the injected dose as assessed by ELISA) (Granowitz *et al.*, 1992). Kim *et al.* (1995) assessed the biodistribution of [^{35}S]IL-1RA in rats in various organs at 3 min post-injection bolus along with the steady-state biodistribution 5 h after i.v. infusion. This animal study demonstrated relatively low uptake [2 and 6% of the injected dose (ID)] in the lung and gut, respectively, but higher uptake in liver (9% ID) and kidney (11% ID) 3 min post-injection. Because kidneys were the only organs with a higher tissue-to-plasma ratio, the authors concluded that kidneys were the preferential route of excretion of IL-1RA. Although Kim *et al.* measured potential metabolites in blood by trichloroacetic acid protein precipitation and HPLC, they only collected data up to 5 min after bolus injection, providing little information on the longer term and more relevant *in vivo* stability of IL-1RA.

As peripheral administration of IL-1RA has been shown to be protective following stroke (Garcia *et al.*, 1995; Relton *et al.*, 1996), although with much higher doses (0.2 to 100 mg kg^{-1} i.v.; 200 mg kg^{-1} s.c.) than is used for centrally administered IL-1RA (usually one administration of 10 μg i.c.v.) (see Touzani *et al.*, 1999), it is still unclear whether actual brain penetration of IL-1RA is required to obtain this protective effect. However, due to the fact that the earliest preclinical studies in stroke models used intracerebroventricular administration (Relton and Rothwell, 1992; Touzani *et al.*, 1999), it seems that intra-parenchymal IL-1RA actions are more potent than peripherally administered IL-1RA. Therefore, Gueorguieva *et al.* (2008) have measured the IL-1RA concentration in the CSF of a group of patients suffering subarachnoid haemorrhage after bolus injection followed by infusion for 24 h. This study showed that the IL-1RA concentration in the CSF was low but comparable with that showing neuroprotective effects in animal models (Relton and Rothwell, 1992; Garcia *et al.*, 1995; Gueorguieva *et al.*, 2008). These data were confirmed later by Clark *et al.* (2008).

Overall, most of the available data concern the plasma pharmacokinetics of IL-1RA, with little published on the biodistribution and more importantly the metabolism of IL-1RA. Here we report the biodistribution and metabolism of ^{18}F-labelled IL-1 receptor antagonist ([^{18}F]IL-1RA) using a novel and rapidly applicable [^{18}F]-radiolabelling technique with a potentially wide scope of applications. The main aim and original contribution of the present study is to investigate in more detail the whole-body biodistribution, pharmacokinetics and metabolism of rhIL-1RA using a new protein radiolabelling technique (Prenant *et al.*, 2008; 2010) and small animal PET.

Methods

Radiosynthesis

[^{18}F]IL-1RA was prepared as described by Prenant *et al.* (2010). For the studies reported here, IL-1RA (typically 2 mg) was

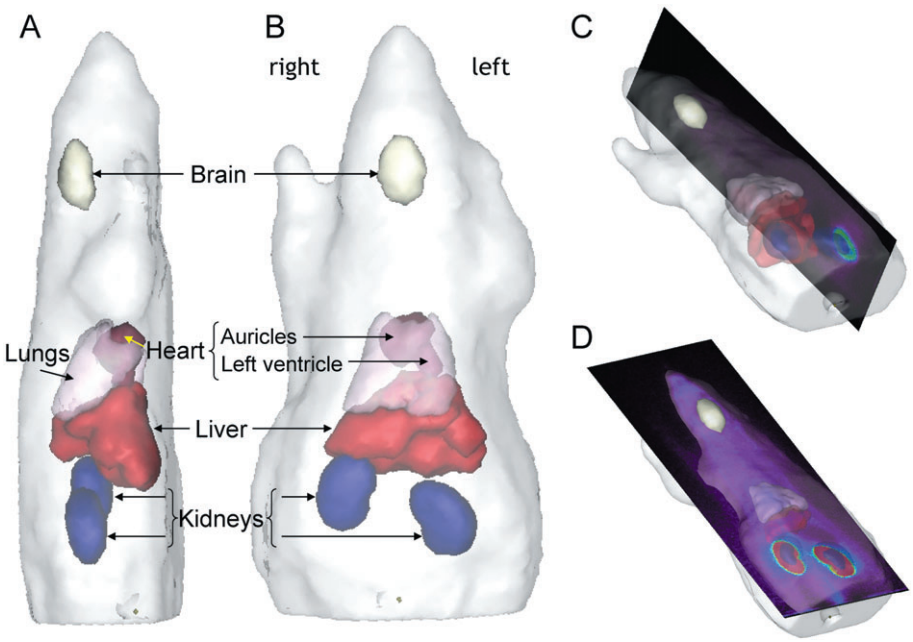

Figure 1

Illustrative 3D view of the automatic segmentation of the organs as carried out with Anatomist software. (A) Sagittal view from the left; (B) axial view from the the top; (C and D) $^{3}/_{4}$ 3D view from the top right with sagittal (C) and longitudinal (D) PET images. 3D animations of parts C and D can be found in the supporting information.

labelled with [^{18}F]fluoroacetaldehyde, which reacts with free amino groups on protein under reductive alkylation conditions, at pH 6 for 45 min at 38°C. The labelled protein was purified using a HiTrap® desalting column (GE Healthcare, Amersham, UK). [^{18}F]IL-1RA, 74.07–311.11 MBq (2.00–8.40 mCi) was collected as a 2 mL fraction. The specific activity ranged from 0.81 to 4.9 GBq μmol^{-1} at the end of the synthesis. QC size exclusion-high performance liquid chromatography (SE-HPLC) analysis, UV absorbance trace (254 nm) as well as the radioactivity trace, showed that the labelled protein was obtained as a pure compound under monomeric and dimeric form, similarly to the reference rhIL-1RA, with a radiochemical purity, for the mixed two forms, over 95%. SDS-PAGE analysis of the labelled rhIL-1RA confirmed the presence of a minor dimeric fraction (faint band at approximately 35 kD), but most of the radioactivity migrated to a position consistent with a 17 kD protein. We have shown previously through the use of autoradiography on rat brain sections that [^{18}F]IL-1RA had retained the ability to bind to its receptor (Prenant *et al.*, 2010).

PET imaging

All animal care and experimental procedures were in accordance with UK legislation under the 1986 Animals (Scientific Procedures) Act. Male Sprague-Dawley rats (300–500 g) were anaesthetized by isoflurane inhalation (induction: 5% and thereafter 2–2.5%) in oxygen and received [^{18}F]IL-1RA in the tail vein (n = 6, injected dose: 12.4~30.5 MBq to 6.96~35.1 nmol; 0.2~2.0 mg kg^{-1}). Respiration and temperature were monitored throughout, using a pressure sensitive pad and rectal probe, Model 1025 L interface and PC-SAM software (SA Instruments, Edison, NJ, USA). Body temperature was maintained by use of a heating pad and a heating and fan module connected to the rectal probe via the interface and controlled by the PC-SAM software. Whole-body images were acquired in list-mode with a non-rotating 16-module quad-HIDAC PET camera for 2 h (Oxford Positron Systems, Weston-on-the-Green, Bicester, UK) with a resolution of 1 mm^3 [Spatial resolution, FWHM (mm), across a cylindrical field of view of 200 mm length and 160 mm diameter: transaxial horizontal 1.02 ± 0.04 mm, transaxial vertical 1.00 ± 0.04 mm, axial: 0.99 ± 0.05 mm, from Hastings *et al.*, 2007]. The list-mode data were reconstructed directly to images (without resorting to histogramming) via the one-pass-list-mode-expectation maximization algorithm (Reader *et al.*, 2002), with one iteration of 16 subsets into images of dimensions 120^2 (transaxially) × 240 (axially) with isotropic 1 mm^3 voxels. Separate reconstructions with 1, 5 and 15 min time framing were performed from which the desired variable time framing were selected and then concatenated in a variable time-frame file (10 × 1 min, 4 × 5 min, 6 × 15 min). Absolute calibration of the images (in kBq cm^{-3}) was achieved by reference to a [^{22}Na] source imaged in the field of view in each scan. This had been validated with a uniformly filled mouse-sized [^{18}F] phantom imaged over 2 h.

Images were segmented using the local means analysis (LMA) method (Maroy *et al.*, 2008) (Figure 1 and Figures S1–S3) and the organ mean time activity curves (TACs) were corrected for partial volume effects. The correction method used combined the geometric transfer matrix (GTM) method and the ROIopt method, both described in Maroy *et al.* (2010). The GTM method requires, in addition to the PET image, spatial domains segmenting homogeneous organs,

provided by the LMA method, and regions of interest (ROIs) for mean TAC computation. This ROI definition method was designed to enhance the robustness of the GTM method to segmentation errors through the automated selection of adequate voxels in the segmented organs. Indeed, the ROIs were defined using the ROIopt method within the LMA segmented regions, although with the number of voxels set to 20% of the number of voxels in the corresponding segmented region. Both methods were applied using the BrainVisa and Anatomist framework.

To account for differences between image and γ–counting data due to activity in the blood, we assumed that PET quantification of [^{18}F]IL-1RA and its metabolites in our ROIs followed a linear superposition of blood and tissue concentrations, for which the following equation applies: $C_{ROI}(t) = fr_{Blood} \times C_{Blood}(t) + C_{Tissue}(t)$, where $C(t)$ is the concentration in [^{18}F]IL-1RA in the ROI, the blood or the tissue and fr_{Blood} is the fraction of blood in each organ. The following correction was thus applied to the PET quantification: $C_{Tissue}(t) = C_{ROI}(t) - fr_{Blood} \times C_{Blood}(t)$ as the amount of blood in each organ is known (Sebestik and Brabec, 1974).

Metabolite study

For the study of IL-1RA metabolites, rats (295–520 g) were killed 20 min, 1 h or 2 h after injection of [^{18}F]IL-1RA (n = 4 per group) (injected dose: 12.4~82.8 MBq to 8.57~66.9 nmol; 0.5~2.6 mg kg^{-1}). Brain, kidneys and liver were quickly removed (1–5 min) and pulverized in liquid nitrogen. Samples of each organ were weighed and counted in a γ-counter. Proteins were extracted by mixing ground sample with lysis buffer (Cell Signalling Technology®, Danvers, MA, USA) containing protease inhibitor cocktail (Sigma-Aldrich, Gillingham, UK) in a 1:1 w/v ratio and centrifuging at 20 000× g for 30 min. For blood and plasma analysis, blood samples (100–200 µL of venous blood) were taken prior to or at death at 1, 5, 10, 20, 60 and 120 min post-injection (n = 3–6 per time-point). Protein assay (BCA protein assay kit: Pierce, Rockford, IL, USA) was performed on samples post-loading and demonstrated uniform loading. In some cases, gels were additionally stained with Coomassie Blue (PhastGel Blue R; GE Healthcare) after autoradiography and loading was shown to be similar. These samples were also used to compare γ-counting of blood samples with PET quantification in the heart cavities (auricle and ventricles). All data were corrected for decay to the time of injection.

Acrylamide gels (15%) were cast with a 4% acrylamide stacking gel using a Mini Protean III system (Bio-Rad, Hercules, CA, USA). Precision Plus Protein Prestained Standards™ (5 µL; Bio-Rad®) were loaded into lane one. Radiolabelled protein and all samples were diluted in 2× Laemlli Buffer (4% SDS, 20% Glycerol, 120 mM Tris.Cl pH 6.8, 0.01% bromophenol blue, 10% 2-mercaptoethanol) and were loaded into lanes 2 and 3 for the [^{18}F]IL-1RA and all other samples into the following lanes. They were run at 100 V (30 mA) until the dye appeared at the bottom, at which point they were removed and fixed by immersion in 45% deionized water, 45% methanol and 10% acetic acid. Gels were then sealed in cling film, photographed and placed into an imaging cassette. Autoradiography was performed using a Fujifilm Bio-Imaging Analyzer BAS-1800II (FujiFilm UK Ltd., Bedford, UK) and data were analysed using Advanced Image Data Analyzer software (Raytest, Straubenhardt, Germany). Radiolabelled protein was sized by overlaying the photograph onto the autoradiogram.

Samples of plasma and urine (25 µL) were analysed by SE-HPLC (as described above).

Statistical analysis

All PET data were expressed as percentage of ID per cubic centimetre (% ID cm^{-3}). Statistical analysis was performed using StatView 5.0 (SAS Institute Inc., Cary, NC, USA). For each ROI (i.e. organs), data uncorrected versus corrected for partial volume effect were compared using a paired non-parametric test of Wilcoxon; PET and γ-counting data were compared using the non-parametric test of Mann–Whitney. For all statistical analysis, the level of significance was $P < 0.05$. All data presented are expressed as mean ± SD.

Materials

Solvents were purchased from Sigma-Aldrich and were used without further purification. The rhIL-1RA, Anakinra® (Kineret®), was kindly provided by Amgen (Thousand Oaks, CA, USA). Anakinra® is a recombinant, methionylated, non-glycosylated synthetic form of the human IL-1RA. It was provided as a solution formulated for injection consisting of 100 mg of Anakinra®, 1.29 mg of sodium citrate, 5.48 mg sodium chloride, 0.12 mg disodium EDTA and 0.70 mg polysorbate 80 in 1 mL water for injection, USP (pH 6.5 at room temperature).

HPLC metabolite and QC analyses of rhIL-1RA and [^{18}F]rhIL-1RA were made by SE-HPLC, performed on an HPLC (Shimadzu UK, Milton Keynes, UK) prominence system operated using a LabLogic software Laura 3 and configured with a CBM-20A controller, a LC-20AB solvent delivery system and a SPD-20A dual wavelength absorbance detector set at 254 and 235 nm. The system was equipped with a Superdex® Gel Filtration Column Peptide HR10/300 GL (GE Healthcare) eluted with phosphate-buffered saline at a 1 mL min^{-1} flow-rate. Radioactivity was monitored with a radio-HPLC Bioscan Flowcount B-FC 3100 detector (Bioscan Europe, Paris, France).

Results

Biodistribution of [^{18}F]IL-1RA assessed by PET imaging and γ-counting

In this study, we focused our quantification of [^{18}F]IL-1RA on the brain as the major organ of interest, along with organs known to be involved in metabolism and excretion, that is, lungs, liver and kidneys (both cortex and medulla). Heart ventricles, which were also identifiable on the PET images, were quantified for comparison with γ-counting of the blood samples.

Our results showed a rapid distribution and elimination of IL-1RA in all organs studied. Overall, as quantified by PET imaging and γ-counting, our data showed low retention in all peripheral organs except the kidneys, in the order: lungs < liver << kidneys (Figure 2A,B and Table 1). In the brain, uptake was even lower than in all peripheral organs (0.11 ± 0.02% ID cm^{-3} 20 min post-injection as quantified by PET

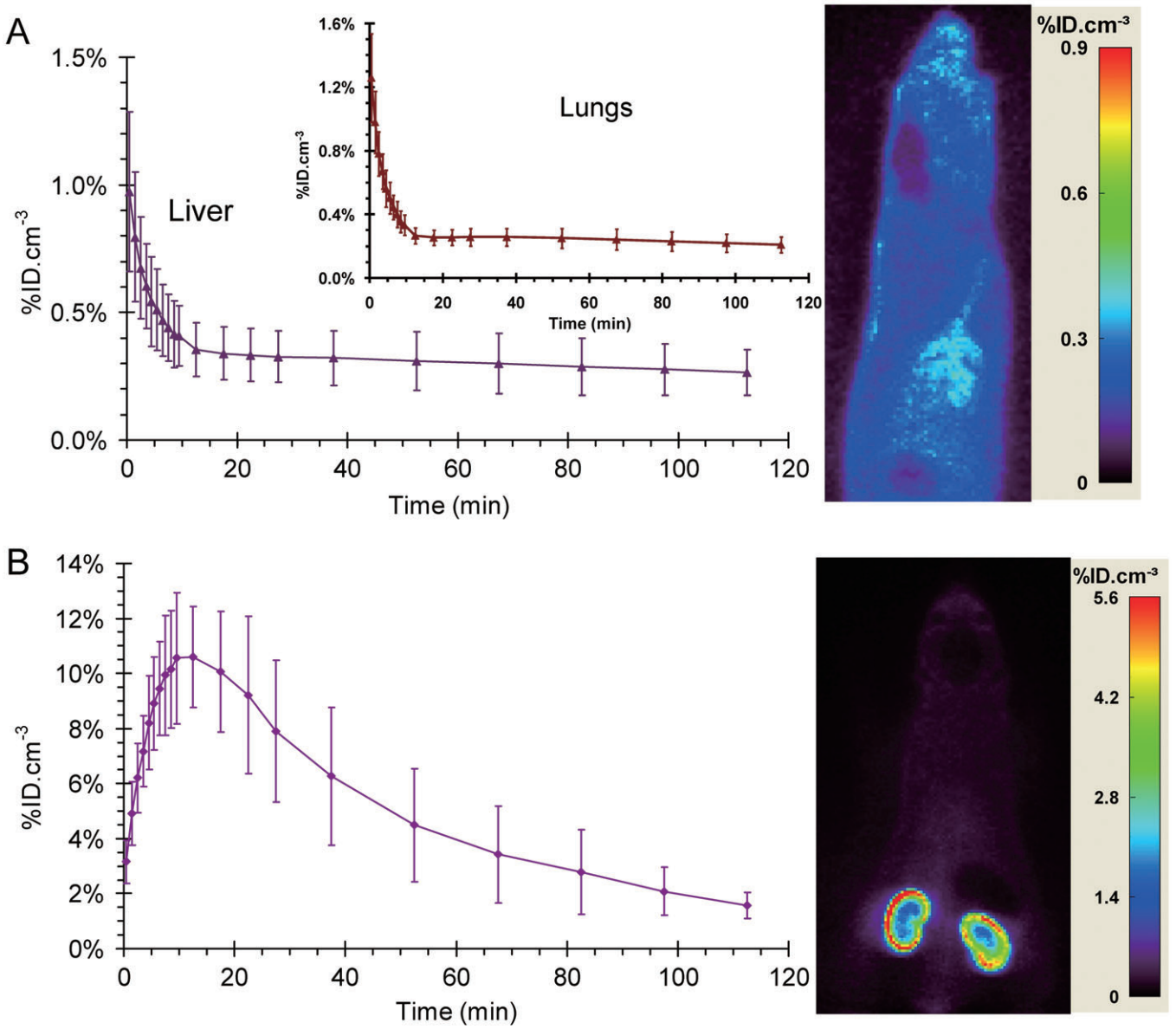

Figure 2

Time-activity curves of [^{18}F]IL-1RA biodistribution (uncorrected for metabolites) and representative summed PET images in liver (A), lungs (A, insert) and kidneys (B).

imaging and 0.02 ± 0.01% ID g^{-1} as quantified by γ-counting) (Figure 3A and Table 1). Interestingly, γ-counting of blood and measurement of heart auricle and ventricle chambers on PET images gave very similar results (Figure 3B and Table 2), with values matching as soon as 5 min post-injection (Figure 3B).

To account for potential partial volume effects, we used the local means analysis-based geometric transfer matrix method (GTM20) as described by Maroy *et al.* (2010). In all organs studied, partial volume effect correction reduced the difference between values obtained from the image and those obtained by γ-counting, improving the accuracy of the PET quantification significantly. In kidneys, for example, partial volume effect correction increased the values obtained from the 60 min time-point image by 24% (2.76 ± 1.25% ID cm^{-3} vs. 3.42 ± 1.77% ID cm^{-3}), making these more comparable with those given by *ex vivo* γ-counting (4.83 ± 0.89% ID cm^{-3}). In light of this, all PET data were corrected for partial volume effects using this method.

As indicated in Table 1, there were discrepancies between PET imaging and γ-counting. PET imaging quantification significantly overestimated [^{18}F]IL-1RA uptake in the brain and liver, whereas it underestimated it in kidneys at 20 min post-injection. In the heart, PET imaging of the heart auricle and ventricles significantly underestimated the blood concentration in [^{18}F]IL-1RA only for the 1 min time-point (Table 2). Importantly though, the relative distribution between organs was consistent (brain << lungs < liver << kidneys).

Table 1
Quantification of [^{18}F]IL-1RA concentration in brain, kidneys and liver by γ-counting and PET imaging, and ratio of PET images to γ-counting quantification

	Brain 20 min	60 min	120 min	Kidneys[a] 20 min	60 min	120 min	Liver 20 min	60 min	120 min
γ-counting	0.02 ± 0.01	0.04 ± 0.00	0.03 ± 0.00	16.7 ± 5.76	4.83 ± 0.89	1.57 ± 0.29	0.18 ± 0.07	0.17 ± 0.02	0.15 ± 0.09
PET (PV corr.)	0.11 ± 0.02*	0.11 ± 0.02*	0.10 ± 0.02*	9.21 ± 2.86*	3.42 ± 1.77	1.58 ± 0.48	0.33 ± 0.10*	0.30 ± 0.12*	0.26 ± 0.09
ratio PET/γ-counting	5.00	2.48	2.99	0.55	0.71	1.00	1.87	1.77	1.73
fr_{Blood}[b]	5%	5%	5%	27%	27%	27%	29%	29%	29%
PET (blood content corr.)	0.09 ± 0.02*†	0.10 ± 0.02*†	0.09 ± 0.02*†	9.14 ± 2.86*	3.36 ± 1.77	1.52 ± 0.48	0.26 ± 0.10†	0.23 ± 0.12†	0.20 ± 0.09
ratio PET/γ-counting	4.39	2.22	2.68	0.55	0.70	0.97	1.45	1.38	1.33

Data are expressed as percentage of injected dose per cm^3, mean ± SD (n = 3–4 per group for γ-counting and n = 6 for PET quantification), PET data were corrected for partial volume effects (Maroy *et al.*, 2010), PET (blood content corr.) = PET data corrected to take into account the fraction of blood (fr_{Blood}) contributing to the PET signal in tissue.
[a]Cortex of the kidneys.
[b]Values from Sebestik and Brabec 1974.
* and †indicate, respectively, significant difference with γ-counting and significant difference (improvement) when compared with the PET (PV corr.) values not corrected for blood fraction, $P < 0.05$. γ-counting versus PET quantification compared using an unpaired Mann–Whitney test, PET (PV. corr.) versus PET (PV and blood content corr.) compared using a paired Wilcoxon test.
PET, positron emission tomography.

Considering the size of IL-1RA (17 kDa), it is likely that (i) only a small amount of intact [^{18}F]IL-1RA will cross the blood brain barrier (BBB) or freely diffuse into other organs; (ii) only metabolites smaller in size will diffuse from the blood into the tissues especially at later time-points; and (iii) considering the low level of expression of IL-1 receptors, specific binding is unlikely to be detectable in most organs. Therefore, a major factor affecting the quality of PET quantification is the contribution of [^{18}F]IL-1RA contained in the blood in each organ; blood that was removed almost entirely during dissection for *ex vivo* γ-counting. To account for this, we assumed that PET quantification of [^{18}F]IL-1RA and its metabolites in our ROIs followed a multi-compartment model (Gueorguieva *et al.*, 2008) in which a correction to account for the contribution of the [^{18}F]IL-1RA contained in the blood was applied (for details see Methods, PET imaging section). In the brain, such corrections significantly improved the measurements when compared with GTM20 PET quantification; however, the PET data were still significantly different from γ-counting at 20, 60 and 120 min time-points (Table 1). Conversely, such corrections did significantly improve the PET quantification in the liver by 22% at 20 and 60 min, in such way that the PET values were no longer significantly different from those derived from γ-counting (Table 1).

As suggested previously by PET and γ-counting quantification, the tissue-to-blood and tissue-to-plasma ratios (Table 3) confirmed that [^{18}F]IL-1RA had a very low uptake in the brain and liver, whereas uptake of [^{18}F]IL-1RA and its metabolites was high in kidneys especially at the early time-point (20 min), with a tissue-to-blood ratio of 60 and tissue-to-plasma ratio of 39 (Table 3), supporting the hypothesis of an important renal excretion of IL-1RA.

Metabolite study

Whereas no metabolites were detectable in the plasma on the HPLC radio-trace at 1, 5 and 10 min post-injection (data not shown), [^{18}F]IL-1RA metabolites became clearly detectable at 20 min post-injection, with about 65% of the [^{18}F]IL-1RA (dimer and monomer) remaining intact while the remainder was cleaved into low molecular weight metabolites (Figure 4C and Table 4). At 60 min post-injection, almost all the [^{18}F]IL-1RA was already metabolized, while at 120 min post-injection no intact IL-1RA was detectable in the plasma (Table 4). In parallel to the metabolism of [^{18}F]IL-1RA as detected by HPLC in the plasma, an increasing proportion of metabolites were detected in the urine (Figure 4D and Table 4). At all time-points, the [^{18}F]IL-1RA consisted of monomer and dimer in plasma, although only the monomer was detectable in urine.

Gel analysis of protein extracts from various organs confirmed a very low level of intact [^{18}F]IL-1RA in the liver, and barely detectable level in the brain; no metabolites were detectable in these organs (Figure 5A–C). In the plasma, as quantified by γ-counting, the level of intact [^{18}F]IL-1RA was relatively low and, in contrast to HPLC analysis, metabolites were not visible on the gels (Figure 5A–C). High levels of both intact [^{18}F]IL-1RA and its metabolites were detected in kidneys (Figure 5A–C). In urine, intact [^{18}F]IL-1RA was detected at 20 min post-injection together with low molecular weight metabolites; at 60 and 120 min post-injection, intact [^{18}F]IL-1RA had become undetectable and almost 100%

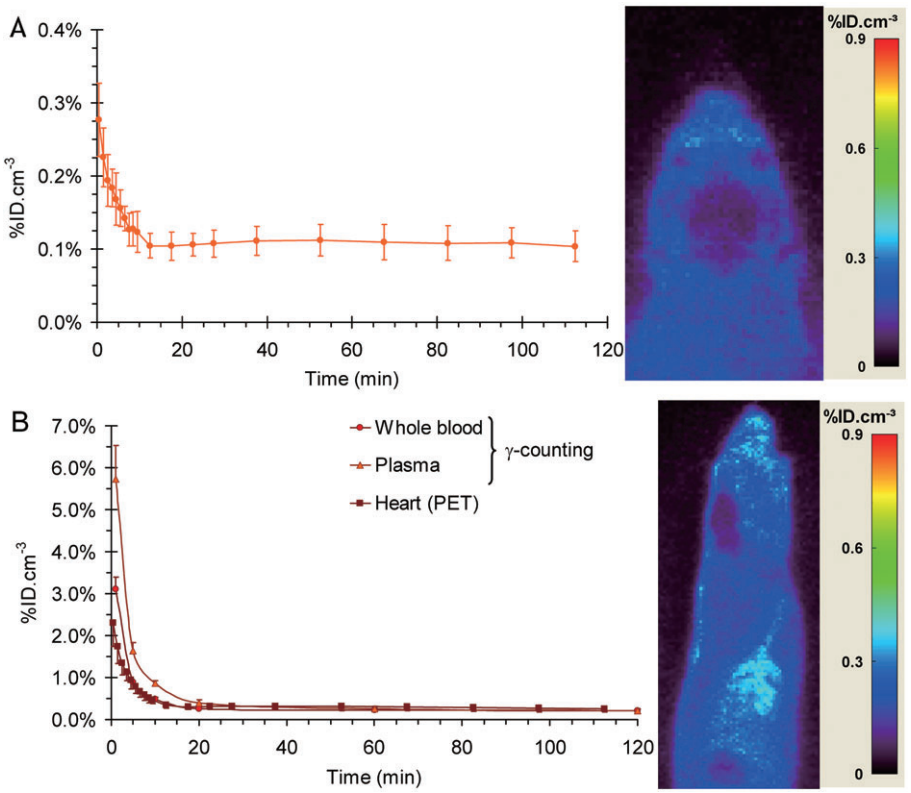

Figure 3

Time-activity curves of [^{18}F]IL-1RA biodistribution (uncorrected for metabolites) and representative summed PET images in the brain (A) and heart (B) compared with data from whole blood (B) and plasma (B) obtained by γ-counting.

Table 2

Plasma and whole-blood concentrations of [^{18}F]IL-1RA and plasma to whole-blood ratios at six time-points following i.v. bolus

	Whole blood 1 min	5 min	10 min	20 min	60 min	120 min
γ-counting	3.11 ± 0.28	0.90 ± 0.02	0.49 ± 0.04	0.26 ± 0.04	0.23 ± 0.04	0.21 ± 0.04
PET (PV corr.)	2.31 ± 0.57*	0.93 ± 0.21	0.48 ± 0.10	0.31 ± 0.07	0.31 ± 0.10	0.26 ± 0.08
ratio PET/γ-counting	0.74	1.04	0.97	1.21	1.35	1.23
	Plasma					
γ-counting	5.73 ± 0.79	1.64 ± 0.19	0.86 ± 0.06	0.40 ± 0.08	0.26 ± 0.05	0.21 ± 0.03
Plasma/whole-blood ratio	1.84 ± 0.18	1.83 ± 0.20	1.76 ± 0.12	1.53 ± 0.11	1.14 ± 0.02	1.00 ± 0.06

Plasma concentrations were assessed only by γ-counting whereas whole-blood was quantified by γ-counting and PET (heart auricle and ventricles were used to assess blood concentration on PET images). PET (not-corr.) = PET data not corrected for partial volume effect, PET (PV corr.) = PET data corrected for partial volume effect (Maroy *et al.*, 2010). Data are expressed as percentage of injected dose per cm^3, mean ± SD (n = 3 to 6 for γ-counting values and n = 6 for PET imaging).
*indicates significant difference with γ-counting; Mann–Whitney test, $P < 0.05$.
PET, positron emission tomography.

of the activity was due to the radiolabelled metabolites (Figure 5D).

We also measured the ratio between plasma and whole-blood [^{18}F]IL-1RA and found that this decreased with time, indicating that the intact molecule was exclusively in plasma at the early time-point (0–10 min post-injection), whereas [^{18}F]IL-1RA metabolites were almost equally distributed between plasma and blood cells at 2 h post-injection

Table 3
Concentration of [^{18}F]IL-1RA in brain, kidneys, liver, plasma and blood quantified by γ-counting, and tissue-to-blood and tissue-to-plasma ratios

	Brain 20 min	60 min	120 min	Kidneys[a] 20 min	60 min	120 min	Liver 20 min	60 min	120 min
γ-counting	0.02 ± 0.01	0.04 ± 0.00	0.03 ± 0.00	16.7 ± 5.76	4.83 ± 0.89	1.57 ± 0.29	0.18 ± 0.07	0.17 ± 0.02	0.15 ± 0.09
Blood γ-counting	0.26 ± 0.04	0.23 ± 0.04	0.21 ± 0.04	0.26 ± 0.04	0.23 ± 0.04	0.21 ± 0.04	0.26 ± 0.04	0.23 ± 0.04	0.21 ± 0.04
Plasma γ-counting	0.40 ± 0.08	0.26 ± 0.05	0.21 ± 0.03	0.40 ± 0.08	0.26 ± 0.05	0.21 ± 0.03	0.40 ± 0.08	0.26 ± 0.05	0.21 ± 0.03
Tissue to blood ratio	0.08 ± 0.05	0.18 ± 0.04	0.17 ± 0.07	60.6 ± 10.5	22.2 ± 7.46	7.65 ± 1.83	0.65 ± 0.17	0.76 ± 0.10	0.72 ± 0.39
Tissue to plasma ratio	0.05 ± 0.03	0.16 ± 0.04	0.17 ± 0.05	40.1 ± 6.86	19.5 ± 6.70	7.63 ± 1.62	0.43 ± 0.09	0.66 ± 0.10	0.72 ± 0.38

γ-Counting data are expressed as percentage of injected dose per cm^3, mean ± SD (n = 3–4 per group). PET data used for the tissue-to-blood and tissue-to-plasma ratio were corrected for partial volume effects.
[a]Cortex of the kidneys.
PET, positron emission tomography.

(Table 3), suggesting metabolites of small molecular weight able to diffuse through the cell membrane and therefore to diffuse in the various organs at later time-points.

Discussion

This work provides new evidence about the biodistribution and metabolism of recombinant human IL-1RA in rodents, and demonstrates the utility of radiolabelling molecules to allow such studies using both PET imaging and γ-counting. Despite the fact that recombinant IL-1RA is in phase II clinical trial for stroke (Emsley *et al.*, 2005) and is used for the treatment of peripheral inflammatory diseases (see Freeman and Buchman, 2001; Barksby *et al.*, 2007), few studies have investigated the biodistribution and pharmacokinetics of IL-1RA and even fewer have reported its metabolism. Such information is nevertheless critical for the optimization of the administration time-points and routes especially as anti-inflammatory strategies have great potential as novel treatments for a broad range of neuropathology.

In this work, we report a relatively low brain penetration (Figure 3A). This is a critical parameter to take into account when planning the treatment of neurodegenerative disease with this molecule, justifying the use of repeated injection or infusion in order to maintain levels compatible with therapeutic efficiency. The brain penetration of IL-1RA reported here (0.02–0.1% ID cm^{-3}) is in agreement with previous reports (Clark *et al.*, 2008; Gueorguieva *et al.*, 2008). Indeed, Clark *et al.* (2008) have shown that although only 0.01% of the injected dose reaches the CSF in both rats and patients, this concentration was effective in significantly reducing the infarct volume in rats. It is worth noting that the BBB is disrupted in stroke, which would lead to higher levels of IL-1RA entering the brain (Greenhalgh *et al.*, 2010). The crossing of the BBB by IL-1RA has been described, although only *in vitro*, as an active process using IL-1 receptors (Skinner *et al.*, 2009). Given that the level of expression of the IL-1 receptors is generally considered to be low and that the amount of IL-1RA injected is high both in our study (up to 2.0 mg kg^{-1}) and in the earlier preclinical and clinical studies (10–200 mg kg^{-1}), it is likely that such mechanism would be saturated by concentrations in this range. It is also worth noting that the route of administration in this study (i.v.) was different from the study by Greenhalgh *et al.* (2010) (subcutaneous), but subcutaneous administration was not compatible with PET imaging particularly in terms of uptake being too slow for the half-life of [^{18}F]; this is also likely to have contributed to differences between studies in the pharmacokinetic of IL-1RA.

In the lungs and liver, our data show here a rapid distribution phase followed by quick washout (Figure 2A and Table 1). Overall, the uptake in liver and lungs is in agreement with the work of Granowitz *et al.* (1992). Similarly, and in line with previous reports, the relatively high uptake in kidneys (Figure 2B) as well as the high tissue-to-plasma ratio of this organ (Table 3) suggest that IL-1RA is metabolized and excreted in this organ (Kim *et al.*, 1995; van der Laken *et al.*, 1998; Barrera *et al.*, 2000); this is also supported by our metabolite study as discussed next. Biodistribution data for IL-1RA labelled with [^{123}I] or [^{125}I] (van der Laken *et al.*, 1996;

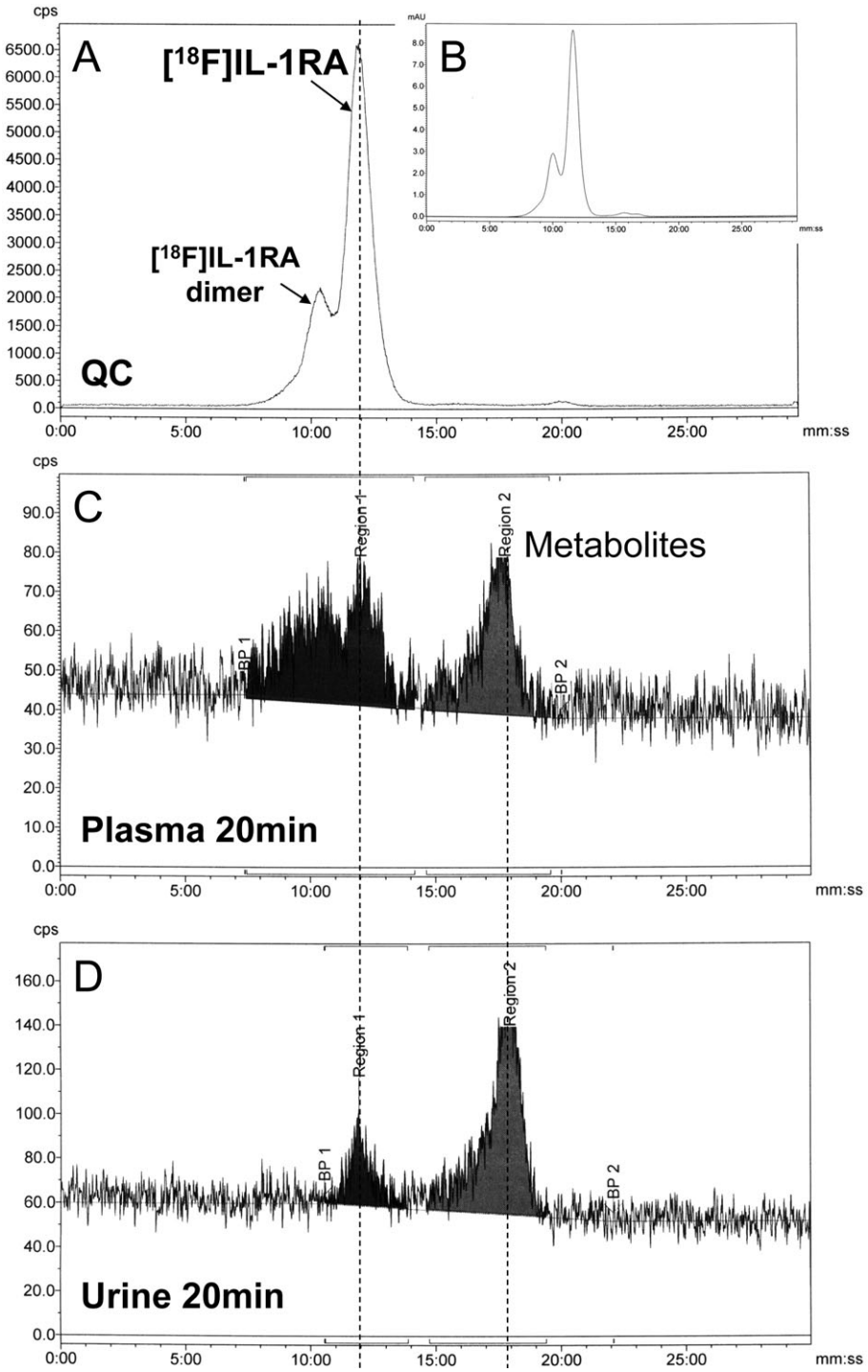

Figure 4

Analysis of [^{18}F]IL-1RA metabolism by SE-HPLC. (A and B): QC of the purified [^{18}F]rhIL-1RA (A, radio-trace; B, UV-trace); (C and D) levels of [^{18}F]-IL-1RA and metabolites at 20 min in plasma (C) and urine (D) (radio-trace).

1998) have been reported and are broadly compatible with our results, although they are not directly comparable considering the difference in the time-points used in these previous reports (4–20 h post-injection).

Here we applied the most recent method developed for the correction of partial volume effects in preclinical PET imaging (Maroy *et al.*, 2010), and this significantly improved our quantification. However, there were still discrepancies between PET and γ-counting quantification, especially in organs with low uptake such as the brain; and various factors can account for this. Firstly, as the basal level of expression of IL-1 receptors has been reported as very low (Dinarello, 1997),

Table 4

Percentage of intact [^{18}F]IL-1RA and metabolites as detected by radio-HPLC 20, 60 and 120 min post-injection (bolus i.v.)

	Plasma 20 min (%)	60 min (%)	120 min (%)	Urine 20 min (%)	60 min (%)	120 min (%)
[^{18}F]IL-1RA	64.5 ± 7.7	15.3 ± 21.7	5.9 ± 8.3	18.3 ± 5.0	11.4 ± 18.3	0.0 ± 0.0
Metabolites	35.5 ± 7.7	84.7 ± 21.7	94.1 ± 8.3	81.7 ± 5.0	88.6 ± 18.3	100.0 ± 0.0

Data are expressed as percentage of the total radioactivity detected in the two peaks of the HPLC radio-trace, mean ± SD (n = 3 to 4 per time-points).

it is likely that there were very few specific binding sites (i.e. IL-1R1 or IL-1R2) expressed in the various organs studied here. Therefore, [^{18}F]IL-1RA concentration as measured by PET imaging was essentially dependent on free diffusion of the molecule and its metabolites at later time-points from the plasma to the tissue, with the blood concentration and perfusion of each organ contributing proportionally to the signal. Correcting for the contribution of the blood volume to the PET signal improved the accuracy of PET measurement in liver significantly, but had limited impact in brain and no effect in kidneys (Table 1). Secondly, it is likely that the lack of scattering correction in the 16-module quad-HIDAC PET camera would account for a significant part of the signal in organs with very low uptake as observed here in the brain. The newer generation of PET scanners can correct for artefacts such as scattering, which particularly affects quantification at low count ranges. In this study, tissue γ-counting of a few *ex vivo* samples was used to check the quantification achieved with PET, thus globally improving the quality of the imaging data. The combination of these techniques when evaluating new radiopharmaceuticals allows time-course studies to be carried out, thus reducing to a minimum the number of animals required.

Here we showed that the excretion of [^{18}F]IL-1RA mainly occurred in kidneys (Figures 3D and 4D). We also showed that no metabolites were detected in the liver, brain and plasma by gel analysis; however, metabolites were detectable in plasma by HPLC, a discrepancy that is likely to be due to the higher amount of activity loaded in the HPLC in comparison with the small amounts loaded on the gels. The excretion through the kidneys of low molecular weight fragments shown here is in agreement with previous reports (Kim *et al.*, 1995; van der Laken *et al.*, 1998; Barrera *et al.*, 2000), although metabolism may occur in the plasma, kidney or a combination of the two. Excretion of large proteins such as IL-1RA in the urine has also been reported (Kim *et al.*, 1995), especially in rats (Gardner, 1961). Moreover, our data demonstrate that this metabolism occurs rapidly as 35.5 ± 7.7% of the [^{18}F]IL-1RA was metabolized within 20 min (Figure 4C and Table 4); this is in agreement with the reported biological half-life of 21 ± 3 min (Granowitz *et al.*, 1992). The low molecular weight of the metabolites is also supported by the plasma to whole-blood ratio which decreased with time, suggesting that intact [^{18}F]IL-1RA remains in the plasma at early time-points whereas metabolites can diffuse into blood cells (Table 3). Radiolabelled [^{18}F]IL-1RA existed largely as a monomer, although some dimerization was detected by HPLC and SDS-PAGE. Therefore, the purity of the administered compound has yet to be confirmed, although we believe that the purity of the compound used here was acceptable for the biodistribution and metabolism study described within this article. It has been shown previously that rhIL-1RA exists in a monomer–dimer equilibrium at relatively high concentrations such as the 100 mg mL^{-1} used in these experiments (Chang *et al.*, 1996; Roy *et al.*, 2005; Alford *et al.*, 2008a,b). Chang *et al.* (1996) also demonstrated that irreversible dimerization occurred, totalling 8% of the total soluble protein, on storage for 2 months at 30°C; the dimer retaining one-third of the bioactivity of the monomer. As our radiolabelling method was applied to other proteins without producing dimerization (data not shown), it may be that the production of the dimer was caused during the storage of the rhIL-1RA. The dimer was present in plasma but not in urine at 20 min (Figure 4C and D), and all other time-points studied which is consistent with differential filtration due to molecular weight.

Our data, taken together with the latest studies of van der Laken (1998) and colleagues (Barrera *et al.*, 2000), suggest that [^{18}F]IL-1RA might be a useful imaging agent for peripheral inflammatory diseases such as chronic rheumatoid arthritis. But interestingly, van der Laken and colleagues did not report on the metabolism of iodine-labelled IL-1RA in their study. The work of these authors leads to the conclusion that radiolabelled IL-1RA could be used as an imaging agent for peripheral inflammatory diseases such as rheumatoid arthritis, but as we showed here the presence of metabolites in plasma would necessitate a correction for accurate image quantification. Moreover, considering that radiolabelled IL-1RA is likely to diffuse relatively slowly then bind to IL-1 receptor in inflamed areas and that the level of IL-1 receptors is known to be extremely low, radiolabelling with longer half-life positron emitter radioisotopes such as [^{124}I] or [^{64}Cu] would be more appropriate. Due to their much longer half-life than [^{18}F], positron emission radioisotopes [^{124}I] (4.2 days) or [^{64}Cu] (12.7 h) have been used for peptides and antibody radiolabelling (Michael and Lewis, 2004), although they both suffer from low positron percentage branching ([^{64}Cu], 18%; ^{124}I, 23%) requiring higher tracer doses to the patient or longer acquisition times in order to obtain good quality PET scans. The complex decay scheme of iodine-124 added to a risk of accumulation of free iodine-124 in the thyroid and stomach, due to de-iodination of the protein, make this radioisotope unsuitable for *in vivo* administration to humans (Linda, 2004; Michael and Lewis, 2004). Copper-64 has found applications

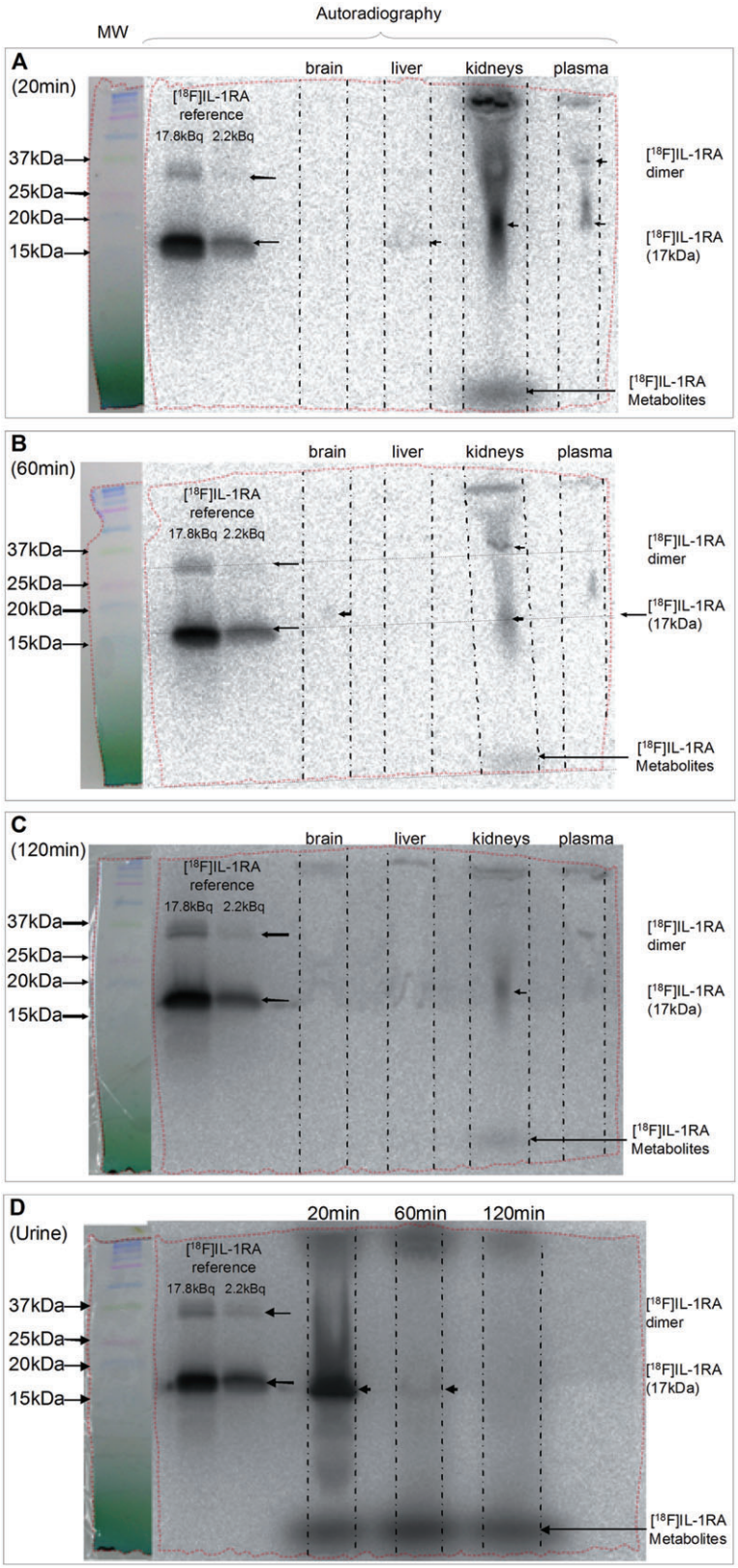

Figure 5

Analysis of [^{18}F]IL-1RA metabolism by SDS-PAGE. (A–C) Levels of [^{18}F]-IL-1RA and metabolites in plasma, liver, brain and kidneys at 20, 60 and 120 min, respectively; (D) time-course of [^{18}F]IL-1RA and metabolites in urine.

in PET/CT imaging, renal perfusion assessments (Green *et al.*, 2007), pancreatic and breast cancer detection (Hoffman and Smith, 2009) as well as cancer therapy (Lewis *et al.*, 2001), and might be a good candidate for IL-1RA labelling.

In conclusion, the combination of PET imaging, via a novel radiolabelling route, and γ-counting allowed us to assess the biodistribution and metabolism of IL-1RA over 2 h. In the present study, we showed low uptake of IL-1RA in the brain, which has consequences for the dosing and administration route of IL-1RA as an anti-inflammatory strategy in the treatment of neurodegenerative disease. We also demonstrated rapid renal metabolism and excretion of IL-1RA, as well as the presence of radiolabelled metabolites in plasma as early as 20 min post-injection, which must be taken into account if radiolabelled IL-1RA is to be used to image chronic peripheral inflammatory diseases. This study illustrates that imaging techniques such as PET can speed up the preclinical assessment of new pharmaceutical agents while reducing the number of animals required. Moreover, this method is generally applicable to proteins using a novel radiolabelling technique.

Acknowledgements

Prof N Rothwell and Dr H Boutin are funded by MRC, UK. Dr C Cawthorne was funded by Cancer Research UK (Grant C153/A4331). The rhIL-1RA (Kineret®/Anakinra®) was generously provided by the Amgen Corporation, but the company was not involved in the design, conduct or analysis of the study. The authors wish to thank the personnel of the Wolfson Molecular Imaging Centre, especially Drs Rainer Hinz and Marie-Claude Asselin for their advices and scientific input, and Messrs Mike Fairclough, Michael Green and Nigel Fry, for facilitating this study. This study was carried out within the EC-FP6 project DiMI (LSHB-CT-2005-512146) framework.

Conflict of interest

N.J.R. is a non-executive director of AstraZeneca, but there was no involvement of the company in any of these studies.

References

Alexander SPH, Mathie A, Peters JA (2009). Guide to Receptors and Channels (GRAC), 4th edn. Br J Pharmacol 158 (Suppl. 1): S1–S254.

Alford JR, Kendrick BS, Carpenter JF, Randolph TW (2008a). High concentration formulations of recombinant human interleukin-1 receptor antagonist: II. Aggregation kinetics. J Pharm Sci 97: 3005–3021.

Alford JR, Kwok SC, Roberts JN, Wuttke DS, Kendrick BS, Carpenter JF *et al.* (2008b). High concentration formulations of recombinant human interleukin-1 receptor antagonist: I. Physical characterization. J Pharm Sci 97: 3035–3050.

Allan SM, Tyrrell PJ, Rothwell NJ (2005). Interleukin-1 and neuronal injury. Nat Rev Immunol 5: 629–640.

Barksby HE, Lea SR, Preshaw PM, Taylor JJ (2007). The expanding family of interleukin-1 cytokines and their role in destructive inflammatory disorders. Clin Exp Immunol 149: 217–225.

Barrera P, van der Laken CJ, Boerman OC, Oyen WJ, Van de Ven MT, van Lent PL *et al.* (2000). Radiolabelled interleukin-1 receptor antagonist for detection of synovitis in patients with rheumatoid arthritis. Rheumatology (Oxford) 39: 870–874.

Bartfai T, Sanchez-Alavez M, Andell-Jonsson S, Schultzberg M, Vezzani A, Danielsson E *et al.* (2007). Interleukin-1 system in CNS stress: seizures, fever, and neurotrauma. Ann N Y Acad Sci 1113: 173–177.

Chang BS, Beauvais RM, Arakawa T, Narhi LO, Dong A, Aparisio DI *et al.* (1996). Formation of an active dimer during storage of interleukin-1 receptor antagonist in aqueous solution. Biophys J 71: 3399–3406.

Clark SR, McMahon CJ, Gueorguieva I, Rowland M, Scarth S, Georgiou R *et al.* (2008). Interleukin-1 receptor antagonist penetrates human brain at experimentally therapeutic concentrations. J Cereb Blood Flow Metab 28: 387–394.

Dinarello CA (1997). Interleukin-1. Cytokine Growth Factor Rev 8: 253–265.

Emsley HC, Smith CJ, Georgiou RF, Vail A, Hopkins SJ, Rothwell NJ *et al.* (2005). A randomised phase II study of interleukin-1 receptor antagonist in acute stroke patients. J Neurol Neurosurg Psychiatry 76: 1366–1372.

Ferrari CC, Pott Godoy MC, Tarelli R, Chertoff M, Depino AM, Pitossi FJ (2006). Progressive neurodegeneration and motor disabilities induced by chronic expression of IL-1beta in the substantia nigra. Neurobiol Dis 24: 183–193.

Freeman BD, Buchman TG (2001). Interleukin-1 receptor antagonist as therapy for inflammatory disorders. Expert Opin Biol Ther 1: 301–308.

Garcia JH, Liu KF, Relton JK (1995). Interleukin-1 receptor antagonist decreases the number of necrotic neurons in rats with middle cerebral artery occlusion. Am J Pathol 147: 1477–1486.

Gardner KDJ (1961). The effect of pH on the filtration, reabsorption, and excretion of protein by the rat kidney. J Clin Invest 40: 525–535.

Godoy MC, Tarelli R, Ferrari CC, Sarchi MI, Pitossi FJ (2008). Central and systemic IL-1 exacerbates neurodegeneration and motor symptoms in a model of Parkinson's disease. Brain 131: 1880–1894.

Granowitz EV, Porat R, Mier JW, Pribble JP, Stiles DM, Bloedow DC *et al.* (1992). Pharmacokinetics, safety and immunomodulatory effects of human recombinant interleukin-1 receptor antagonist in healthy humans. Cytokine 4: 353–360.

Green MA, Mathias CJ, Willis LR, Handa RK, Lacy JL, Miller MA *et al.* (2007). Assessment of Cu-ETS as a PET radiopharmaceutical for evaluation of regional renal perfusion. Nucl Med Biol 34: 247–255.

Greenhalgh AD, Galea J, Denes A, Tyrrell PJ, Rothwell NJ (2010). Rapid brain penetration of interleukin-1 receptor antagonist in rat cerebral ischaemia: pharmacokinetics, distribution, protection. Br J Pharmacol 160: 153–159.

Grierson JR, Yagle KJ, Eary JF, Tait JF, Gibson DF, Lewellen B *et al.* (2004). Production of [F-18]fluoroannexin for imaging apoptosis with PET. Bioconjug Chem 15: 373–379.

Gueorguieva I, Clark SR, McMahon CJ, Scarth S, Rothwell NJ, Tyrrell PJ *et al.* (2008). Pharmacokinetic modelling of interleukin-1 receptor antagonist in plasma and cerebrospinal fluid of patients following subarachnoid haemorrhage. Br J Clin Pharmacol 65: 317–325.

Hastings DL, Reader AJ, Julyan PJ, Zweit J, Jeavons AP, Jones T (2007). Performance characteristics of a small animal PET camera for molecular imaging. Nucl Instrum Methods Phys Res A 573: 80–83.

Haubner R, Wester HJ, Weber WA, Mang C, Ziegler SI, Goodman SL *et al.* (2001). Noninvasive imaging of alpha(v)beta3 integrin expression using 18F-labeled RGD-containing glycopeptide and positron emission tomography. Cancer Res 61: 1781–1785.

Hoffman TJ, Smith CJ (2009). True radiotracers: Cu-64 targeting vectors based upon bombesin peptide. Nucl Med Biol 36: 579–585.

Holmes C, El-Okl M, Williams AL, Cunningham C, Wilcockson D, Perry VH (2003). Systemic infection, interleukin 1beta, and cognitive decline in Alzheimer's disease. J Neurol Neurosurg Psychiatry 74: 788–789.

Kavanaugh A (2006). Anakinra (interleukin-1 receptor antagonist) has positive effects on function and quality of life in patients with rheumatoid arthritis. Adv Ther 23: 208–217.

Kim DC, Reitz B, Carmichael DF, Bloedow DC (1995). Kidney as a major clearance organ for recombinant human interleukin-1 receptor antagonist. J Pharm Sci 84: 575–580.

Kramer-Marek G, Kiesewetter DO, Martiniova L, Jagoda E, Lee SB, Capala J (2008). [18F]FBEM-Z(HER2:342)-Affibody molecule-a new molecular tracer for in vivo monitoring of HER2 expression by positron emission tomography. Eur J Nucl Med Mol Imaging 35: 1008–1018.

van der Laken CJ, Boerman OC, Oyen WJ, Van de Ven MT, Claessens RA, van der Meer JW *et al.* (1996). Different behaviour of radioiodinated human recombinant interleukin-1 and its receptor antagonist in an animal model of infection. Eur J Nucl Med 23: 1531–1535.

van der Laken CJ, Boerman OC, Oyen WJ, Van de Ven MT, van der Meer JW, Corstens FH (1998). Imaging of infection in rabbits with radioiodinated interleukin-1 (alpha and beta), its receptor antagonist and a chemotactic peptide: a comparative study. Eur J Nucl Med 25: 347–352.

Lee BC, Ahn SY, Doo HK, Yim SV, Lee HJ, Jin SY *et al.* (2004). Susceptibility for ischemic stroke in Korean population is associated with polymorphisms of the interleukin-1 receptor antagonist and tumor necrosis factor-alpha genes, but not the interleukin-1beta gene. Neurosci Lett 357: 33–36.

Lewis J, Laforest R, Buettner T, Song S, Fujibayashi Y, Connett J *et al.* (2001). Copper-64-diacetyl-bis(N4-methylthiosemicarbazone): an agent for radiotherapy. Proc Natl Acad Sci USA 98: 1206–1211.

Linda CK (2004). Radiolabeled peptides for tumor imaging. In: Welch MJ, Redvanly CS (eds). Handbook of Radiopharmaceuticals. John Wiley & Sons, Ltd: Chichester, UK, pp. 643–684.

Lucas SM, Rothwell NJ, Gibson RM (2006). The role of inflammation in CNS injury and disease. Br J Pharmacol 147 (Suppl. 1): S232–S240.

McColl BW, Allan SM, Rothwell NJ (2009). Systemic infection, inflammation and acute ischemic stroke. Neuroscience 158: 1049–1061.

Maroy R, Boisgard R, Comtat C, Frouin V, Cathier P, Duchesnay E *et al.* (2008). Segmentation of rodent whole-body dynamic PET images: an unsupervised method based on voxel dynamics. IEEE Trans Med Imaging 27: 342–354.

Maroy R, Boisgard R, Comtat C, Jego B, Fontyn Y, Jan S *et al.* (2010). Quantitative organ time activity curve extraction from rodent PET images without anatomical prior. Med Phys 37: 1507–1517.

Michael RZ, Lewis JS (2004). Radiolabeled antibodies for tumor imaging and therapy. In: Welch MJ, Redvanly CS (eds). Handbook of Radiopharmaceuticals. John Wiley & Sons, Ltd: Chichester, UK, pp. 685–714.

Mogi M, Harada M, Kondo T, Riederer P, Inagaki H, Minami M *et al.* (1994). Interleukin-1 beta, interleukin-6, epidermal growth factor and transforming growth factor-alpha are elevated in the brain from Parkinsonian patients. Neurosci Lett 180: 147–150.

Neven B, Marvillet I, Terrada C, Ferster A, Boddaert N, Couloignier V *et al.* (2010). Long-term efficacy of the interleukin-1 receptor antagonist anakinra in ten patients with neonatal-onset multisystem inflammatory disease/chronic infantile neurologic, cutaneous, articular syndrome. Arthritis Rheum 62: 258–267.

Pinteaux E, Rothwell NJ, Boutin H (2006). Neuroprotective actions of endogenous interleukin-1 receptor antagonist (IL-1ra) are mediated by glia. Glia 53: 551–556.

Prenant C, Gillies J, Bailey J, Chimon G, Smith N, Jayson GC *et al.* (2008). Synthesis of [^{18}F]fluoroacetaldehyde. Application to [^{18}F]fluoroethylation of benzylamine under reductive alkylation conditions. J Labelled Comp Radiopharm 51: 262–267.

Prenant C, Cawthorne C, Fairclough M, Rothwell N, Boutin H (2010). Radiolabeling with fluorine-18 of a protein, interleukin-1 receptor antagonist. Appl Radiat Isot 68: 1721–1727.

Reader AJ, Ally S, Bakatselos F, Manavaki R, Walledge RJ, Jeavons AP *et al.* (2002). One-pass list-mode EM algorithm for high-resolution 3-D PET image reconstruction into large arrays. IEEE Trans Nucl Sci 49: 693–699.

Relton JK, Rothwell NJ (1992). Interleukin-1 receptor antagonist inhibits ischaemic and excitotoxic neuronal damage in the rat. Brain Res Bull 29: 243–246.

Relton JK, Martin D, Thompson RC, Russell DA (1996). Peripheral administration of interleukin-1 receptor antagonist inhibits brain damage after focal cerebral ischemia in the rat. Exp Neurol 138: 206–213.

Roy S, Jung R, Kerwin BA, Randolph TW, Carpenter JF (2005). Effects of benzyl alcohol on aggregation of recombinant human interleukin-1-receptor antagonist in reconstituted lyophilized formulations. J Pharm Sci 94: 382–396.

Schottelius M, Wester HJ (2009). Molecular imaging targeting peptide receptors. Methods 48: 161–177.

Sebestik V, Brabec V (1974). Red cell, plasma and whole blood volumes in organs of normal and hypersplenic rats. Blut 29: 203–209.

Shaftel SS, Kyrkanides S, Olschowka JA, Miller JN, Johnson RE, O'Banion MK (2007). Sustained hippocampal IL-1beta overexpression mediates chronic neuroinflammation and ameliorates Alzheimer plaque pathology. J Clin Invest 117: 1595–1604.

Shaftel SS, Griffin WS, O'Banion MK (2008). The role of interleukin-1 in neuroinflammation and Alzheimer disease: an evolving perspective. J Neuroinflammation 5: 1742–2094.

Simi A, Tsakiri N, Wang P, Rothwell NJ (2007). Interleukin-1 and inflammatory neurodegeneration. Biochem Soc Trans 35: 1122–1126.

Skinner RA, Gibson RM, Rothwell NJ, Pinteaux E, Penny JI (2009). Transport of interleukin-1 across cerebromicrovascular endothelial cells. Br J Pharmacol 156: 1115–1123.

Tansey MG, McCoy MK, Frank-Cannon TC (2007). Neuroinflammatory mechanisms in Parkinson's disease: potential environmental triggers, pathways, and targets for early therapeutic intervention. Exp Neurol 208: 1–25.

Touzani O, Boutin H, Chuquet J, Rothwell N (1999). Potential mechanisms of interleukin-1 involvement in cerebral ischaemia. J Neuroimmunol 100: 203–215.

Vezzani A, Balosso S, Maroso M, Zardoni D, Noe F, Ravizza T (2010). ICE/caspase 1 inhibitors and IL-1beta receptor antagonists as potential therapeutics in epilepsy. Curr Opin Investig Drugs 11: 43–50.

Wester H, Schottelius M (2007). Fluorine-18 labeling of peptides and proteins. In: Schubiger PA, Lehmann L, Friebe M (eds). PET Chemistry, the Driving Force in Molecular Imaging. Springer: Berlin, Heidelberg, pp. 79–111.

Wester HJ, Schottelius M, Scheidhauer K, Meisetschlager G, Herz M, Rau FC *et al*. (2003). PET imaging of somatostatin receptors: design, synthesis and preclinical evaluation of a novel 18F-labelled, carbohydrated analogue of octreotide. Eur J Nucl Med Mol Imaging 30: 117–122.

Yagle KJ, Eary JF, Tait JF, Grierson JR, Link JM, Lewellen B *et al*. (2005). Evaluation of 18F-annexin V as a PET imaging agent in an animal model of apoptosis. J Nucl Med 46: 658–666.

Supporting information

Additional Supporting Information may be found in the online version of this article:

Figure S1 3D animation of the longitudinal view of the PET images and its automatic segmentation from Figure 1.
Figure S2 3D animation of the sagittal view of the PET images and its automatic segmentation from Figure 1.
Figure S3 3D animation of the projection view of the PET images and its automatic segmentation from Figure 1.

Please note: Wiley-Blackwell are not responsible for the content or functionality of any supporting materials supplied by the authors. Any queries (other than missing material) should be directed to the corresponding author for the article.